Atmos. Chem. Phys. Discuss., 11, 13723–13767, 2011
www.atmos-chem-phys-discuss.net/11/13723/2011/
doi:10.5194/acpd-11-13723-2011
© Author(s) 2011. CC Attribution 3.0 License.

Atmospheric Chemistry and Physics Discussions

This discussion paper is/has been under review for the journal Atmospheric Chemistry and Physics (ACP). Please refer to the corresponding final paper in ACP if available.

Carbon monoxide (CO) and ethane (C_2H_6) trends from ground-based solar FTIR measurements at six European stations, comparison and sensitivity analysis with the EMEP model

J. Angelbratt[1], J. Mellqvist[1], D. Simpson[1,2], J. E. Jonson[2], T. Blumenstock[6], T. Borsdorff[5], P. Duchatelet[3], F. Forster[5], F. Hase[6], E. Mahieu[3], J. Notholt[4], A. K. Petersen[4,*], U. Raffalski[6], C. Servais[3], R. Sussman[5], and T. Warneke[4]

[1]Chalmers University of Technology, Göteborg, Sweden
[2]EMEP MSC-W, Norwegian Meteorological Institute, Oslo, Norway
[3]Institute of Astrophysics and Geophysics, University of Liège, Liège, Belgium
[4]Institute of Environmental Physics, University of Bremen, Bremen, Germany
[5]Karlsruhe Institute of Technology (KIT), Institute for Meteorology and Climate Research (IMK-ASF), Garmisch-Patenkirchen, Germany

[6]Karlsruhe Institute of Technology (KIT), Institute for Meteorology and Climate Research (IMK-ASF), Karlsruhe, Germany
[*]present address: Max-Planck-Institute for Meteorology, Hamburg, Germany

Received: 22 March 2011 – Accepted: 21 April 2011 – Published: 5 May 2011

Correspondence to: J. Mellqvist (johan.mellqvist@chalmers.se)

Published by Copernicus Publications on behalf of the European Geosciences Union.

ACPD
11, 13723–13767, 2011

Abstract

Trends in the CO and C_2H_6 partial columns (~0–15 km) have been estimated from four European ground-based solar FTIR stations for the 1996–2006 time period. The CO trends from the four stations Jungfraujoch, Zugspitze, Harestua and Kiruna have been estimated to $-0.45\pm0.16\,\%\,yr^{-1}$, $-1.00\pm0.24\,\%\,yr^{-1}$, $-0.62\pm0.19\,\%\,yr^{-1}$ and $-0.61\pm0.16\,\%\,yr^{-1}$, respectively. The corresponding trends for C_2H_6 are $-1.51\pm0.23\,\%\,yr^{-1}$, $-2.11\pm0.30\,\%\,yr^{-1}$, $-1.09\pm0.25\,\%\,yr^{-1}$ and $-1.14\pm0.18\,\%\,yr^{-1}$. To find possible reasons for the CO trends, the global-scale EMEP MSC-W chemical transport model has been used in a series of sensitivity scenarios. It is shown that the trends are consistent with the combination of a 20 % decrease in the anthropogenic CO emissions seen in Europe and North America during the 1996-2006 period and a 20 % increase in the anthropogenic CO emissions in East Asia, during the same time period. The possible impacts of CH_4 and biogenic volatile organic compounds (BVOCs) are also considered. The European and global-scale EMEP model have been evaluated against the measured CO and C_2H_6 partial columns from Jungfraujoch, Zugspitze, Bremen, Harestua, Kiruna and Ny-Ålesund. The European model reproduces, on average the measurements at the different sites fairly well and within 10–22 % deviation for CO and 14–31 % deviation for C_2H_6. Their seasonal amplitude is captured within 6–35 % and 9–124 % for CO and C_2H_6, respectively. However, 61–98 % of the CO and C_2H_6 partial columns in the European model are shown to arise from the boundary conditions, making the global-scale model a more suitable alternative when modeling theses two species. In the evaluation of the global model the average partial columns for year 2006 have shown to be within 1–9 % and 37–50 % for CO and C_2H_6, respectively. The global model sensitivity for assumptions done in this paper is also analyzed.

ACPD
11, 13723–13767, 2011

1 Introduction

During the last 30 years the trend in tropospheric carbon monoxide (CO) has turned from positive in the 1980s, to negative, in the 1990s and 2000s. The trend in the Northern Hemisphere has changed from approximately a 1 % increase per year to a decrease of 1–1.5 % per year with the strongest negative trends reported at high northern latitudes (Khalil and Rasmussen, 1988, 1994; Novelli et al., 2003). In contrast, ethane (C_2H_6) has shown a constant negative trend in both the 1980s and 1990s of roughly 1–3 % per year (Rinsland et al., 1998; Mahieu et al., 1997).

These changes are important as tropospheric chemistry to a large extent is controlled by the hydroxyl (OH) radical, also often referred to as the detergent of the atmosphere. One of the main OH sinks is the reaction with CO (Crutzen et al., 1999). In this oxidation, the greenhouse gas carbon dioxide is formed but the reaction is also related to the formation or destruction of tropospheric ozone (O_3), depending on the NO_x concentrations in the ambient air. C_2H_6 is the second most common organic trace gas in the troposphere after methane (CH_4) and is, like CO, destroyed by the OH radical. C_2H_6 has also shown to be a major route for the formation of peroxyacetyl nitrate (PAN) which acts as a NO_x reservoir and thereby accelerates O_3 formation in the troposphere (Blake and Rowland, 1986; Finlayson-Pitts and Pitts, 2000).

Trends in the concentration of CO and C_2H_6 as seen from a particular location can result from both changes in emissions and changes in chemical production and loss processes. Observations alone cannot usually distinguish between these factors. In principal, chemical transport models (CTMs) can account for all the major processes affecting CO and C_2H_6, but such models are also limited by both inherent deficiencies and not least by the quality of the emissions data upon which such models rely.

The purpose of this paper is to make use of one such CTM, the global-scale EMEP MSC-W model, to explore the trends seen in ground-based solar FTIR measurements of CO from four European stations. This is done in a sensitivity analysis covering a series of scenarios based on changes in the anthropogenic CO emissions and in the

ACPD
11, 13723–13767, 2011

global temperature and methane concentration. The FTIR dataset used in this paper are compiled within the NDACC network (Network for the Detection of Atmospheric Composition Change, http://ndacc.org/) for which a wide range of atmospheric species is measured in the mid infrared spectral region with high resolution spectrometers, generally since the early 1990s, and even the mid-1980s at Jungfraujoch. An important part of the current study is also to evaluate how well the EMEP model reproduces observed CO and C_2H_6 levels, both as an opportunity to evaluate this model using novel measurements, and to give confidence to the use of the model for such sensitivity analysis. It can be noted that many comparisons between CTMs and satellite and in situ measurements regarding CO have been performed earlier but often with poor results, especially in the spring time maxima (Isaksen et al., 2009; Shindell et al., 2006).

2 Chemistry and sources of CO and C_2H_6

CO concentrations in the atmosphere are affected by emissions and chemical formation. Primary emissions of CO result from incomplete combustion of carbon-containing fuels. In developed countries the major anthropogenic source is related to emissions from the transport sector (Finlayson-Pitts and Pitts, 2000). Natural CO sources include oxidation from organics, primarily from atmospheric methane and biogenic hydrocarbons (BVOC), and from biological processes in soils and ocean. An overview of the estimated global CO sources is presented in Table 1, where also the contribution from biomass burning is included. In Table 1 it can be seen that the major source for CO is the natural one and that the anthropogenic source globally only contributes to approximately 15 % of the total yearly emissions. Almost all of the CO emissions from fossil fuel combustion and 2/3 of the biomass burning are located in the Northern Hemisphere (Holloway et al., 2000). The CO source from oxidation of biogenic hydrocarbons is roughly equally divided between the hemispheres and that from methane oxidation is slightly higher in the Northern Hemisphere. The major CO sink is the reaction with

ACPD
11, 13723–13767, 2011

the OH radical, seen in Reaction (R1), accounting for 90–95 % of the total CO loss (Lelieveld et al., 2002). CO is also a key compound in the formation and destruction of tropospheric O_3 depending on the background concentrations of NO_x (Crutzen et al., 1999).

$$CO + OH(+O_2) \rightarrow HO_2 + CO_2 \quad \text{(R1)}$$

In the Northern Hemisphere, Reaction (R1) is the dominant sink for OH, and even in polluted European boundary layers, CO accounts for significant fractions of OH loss (Simpson et al., 1995). The OH radical is produced from photo dissociation of O_3 ($\lambda \leq 0.32\,\mu m$) and water according to Reactions (R2) and (R3), respectively. Since the formation of the OH radical is strongly dependent of the amount of sunlight, the CO concentration shows a strong intra annual behavior with low values in the summer and high in the winter.

$$O_3 + h\nu \rightarrow O_2 + O(^1D) \quad \text{(R2)}$$

$$O(^1D) + H_2O \rightarrow 2OH \quad \text{(R3)}$$

In Reaction (R3) only a small fraction of the energetically excited oxygen atoms, $O(^1D)$, ($\approx$10 %) react with water molecules and produce OH, the others recombine with O_2 to form O_3 (Finlayson-Pitts and Pitts, 2000).

The main C_2H_6 source is of anthropogenic origin and includes production and transport of fossil fuels and use of bio fuel. Another important source is biomass burning (Xiao et al., 2008, Table 1). Xiao et al. (2008) also estimates the anthropogenic and biomass burning emissions in Europe to 2.1 and $<0.1\,Tg\,yr^{-1}$, respectively. As much as 84 % of the C_2H_6 sources are located on the Northern Hemisphere with highest emissions in Asia followed by North America and Europe. The main sink, which causes up to 95 % of the C_2H_6 removal, is the reaction with the OH radical in which the ethyl radical and water are formed, see Reaction (R4).

$$C_2H_6 + OH \rightarrow C_2H_5 + H_2O \quad \text{(R4)}$$

ACPD
11, 13723–13767, 2011

The ethyl radical is then transformed through a complicated pattern of oxidations and reductions and ultimately ends up as CO (Aikin et al., 1982).

3 FTIR measurements

In this paper, FTIR partial columns data of CO and C_2H_6 from six European stations are used from the time period of 1996–2006. Information regarding the FTIR stations can be found in Table 2.

A column is defined as the integrated amount of a species from the measurement station to a certain altitude, usually expressed as the number of molecules per unit area (molecules cm^{-2}). When retrieving data from solar FTIR measurements, a synthetic spectrum is calculated in a forward model in which the atmosphere is divided into discrete layers. To compute the synthetic spectrum, a priori vertical distributions, line parameters for the target and interfering gases as well as temperature- and pressure profiles are needed. To account for line broadening caused by the spectrometer, the instrument lineshape is included in the calculation. The synthetic spectrum is then compared with the measured one and the forward model parameters are adjusted in an iterative way until the modeled spectrum is sufficiently close to the measured one. This inverse process is an ill posed problem that is solved with the Optimal Estimation Method (OEM) in which the final retrieved profile is a weight of an a priori profile of the target gas and the measurement (Rodgers, 2000). In order to use the OEM method, uncertainties in the a priori profile and measurements have to be assumed/known. The partial column is obtained by multiplying the retrieved profile with a pressure profile and sum the result to the height of interest. The retrieval procedure is implemented in an algorithm called SFIT2 (Rinsland et al., 1998) which is used for all the participating stations except Kiruna, which use PROFFIT. These two algorithms have shown to be within 1 % agreement (Hase et al., 2004; Duchatelet et al., 2010). The micro windows used in the present retrievals is in the region from 2057 to 2159 cm^{-1} for CO and from 2976 to 2977 cm^{-1} for C_2H_6. For, CO the species O_3, H_2O, CO_2, N_2O and OCS act

ACPD
11, 13723–13767, 2011

as interfering species while CH_4, O_3 and H_2O interact with C_2H_6. The retrieval strategy used for CO and C_2H_6 was developed within the UFTIR (http://www.nilu.no/uftir/) project and are further described by De Maziere (2005) and Vigouroux et al. (2008). Errors for the measured tropospheric column (0.2–12 km) above a Japanese site has been estimated by Zhao et al. (2002) and found to be 6.7 % and 8.4 % for CO and C_2H_6, respectively. The instrumental line shapes at all stations are monitored with gas cells measurements on a regular basis. These measurement are retrieved with the LINEFIT program developed by Hase et al. (1999) and used to adjust for the line broadening in the retrievals.

4 The EMEP model

The European Monitoring and Evaluation Programme (EMEP, www.emep.int) started in 1977, a successful effort between almost all European countries to pool efforts in tackling the major environmental problem of the day, acid deposition. When the Convention on Long-range Transboundary Air Pollution (CLRTAP, www.unece.org/env/lrtap) was established in 1979, EMEP became an integrated part of the Convention, and has since played an important part in the development of emission reductions scenarios, for both the Convention (now comprising 51 Parties, including USA and Canada) and the European Commission.

The EMEP Chemical Transport model (CTM) (Simpson et al., 2003a; 2010) is a development of the 3-D chemical transport model of Berge and Jakobsen (1998), extended with photo-oxidant chemistry (Simpson et al., 1995, 2003b; Andersson-Skold and Simpson, 1999) and the EQSAM gas/aerosol partitioning model (Metzger et al., 2002). Traditionally, this model has been run in a domain centered over Europe, but also covering large parts of the North Atlantic. The European-scale model has a resolution of about $50 \times 50\,km^2$, true at 60° N polar stereographic projection, and extending vertically from ground level to the tropopause and the lower stratosphere (100 hPa). The model has undergone substantial development in recent years, and is now ap-

ACPD
11, 13723–13767, 2011

plied on scales ranging from local (ca. 5 km grid size, Vieno et al., 2010) to global (with 1 degree resolution, (Jonson et al., 2010)). The model presented in this paper uses version rv3.5 of EMEP model, see Simpson et al. (2010). Both natural and anthropogenic emissions are included. The anthropogenic emissions are provided by most European countries on the 50×50 km^2 grid, otherwise derived from global databases or expert estimates. Biogenic emissions of isoprene in Europe are based on Guenther et al. (1993) and Simpson et al. (1999), driven by landcover for the appropriate grid. Emissions from forest-fires are available as 8-day averages from the GFED (Global Emission Fire Database) database of van der Werf (2006). Unfortunately these data do not cover the full 1996-2006 period of our trend-runs, so we run the European-scale version of the model without forest fires, and evaluate their impact for 2006 with the global version.

When run at the European scale, initial and boundary values are required for the important long-lived pollutants, notably O_3, CH_4, CO and some hydrocarbons including C_2H_6. Concentrations of O_3 are most crucial to the model's photochemical calculations, and these are derived from climatological data of Logan et al. (1999), modified with a so-called Mace-Head correction to correct for observed monthly background O_3 changes (Simpson et al., 2003c). CO and C_2H_6 are specified as simple functions of latitude, altitude and time-of-year. The values were chosen to loosely reproduce observations from a number of studies (e.g. Derwent et al., 1998; Ehhalt et al., 1991; Emmons et al., 2000; Warneck, 2000) and the equations for the boundary condition calculations for CO and C_2H_6 are presented in Eqs. (1) and (2).

$$C_0 = C_{\text{mean}} + \Delta C \cdot \cos\left(2\pi \frac{(d_{\text{mm}} - d_{\text{max}})}{n_y}\right) \quad (1)$$

The CO and C_2H_6 concentration at ground-level (C_0) are calculated as a function of the average concentration (C_{mean}), the amplitude (ΔC) and the phase where d_{mm} is the mid month number, d_{max} is the day at which C_0 maximizes and n_y is the number of days each year. Vertical (profile) concentrations are calculated according to Eq. (2).

ACPD
11, 13723–13767, 2011

Where h is the height and H_z is the scale height with 10 km used for C_2H_6 and 25 km for CO.

$$C_i(h) = C_0 \exp(-h/H_z) \quad (2)$$

The parameters used in Eqs. (1) and (2) can be found in Simpson et al. (2003c).

The European EMEP model has been compared with observations and trends in several studies. Jonson et al. (2006) examined trends in ground-level ozone, Simpson et al. (2006) looked at deposition fluxes of sulphur and nitrogen, Fagerli et al. (2007) compared historical trends of sulphate, ammonium and elemental carbon against ice-core records in the Alps, and Fagerli and Aas (2008) examined trends in nitrogen compounds in air and precipitation from 1980–2003.

In recent years the EMEP model has been extended to run at the hemispheric and global- scales. Indeed, calculated results with an earlier hemispheric version of the model have been uploaded to the HTAP database (www.htap.org). More than 30 models have uploaded model calculations for the year 2001 on this database, with model intercomparisons and comparison with measurements reported in several studies (HTAP, 2007; Fiore et al., 2009; Shindell et al., 2008; Sanderson et al., 2008; Reidmiller et al., 2009; Jonson et al., 2010). In general the EMEP performs well compared to the other models in the database for surface species and depositions. In the free troposphere the EMEP model tended to underpredict ozone in the summer months compared to other models and to measurements (Jonson et al., 2006). Since this HTAP study, changes have been made to the advection scheme (in particular with the inclusion of a convection scheme for dealing with e.g. sub-grid cumulus clouds), and ozone levels in the free troposphere are now higher, and in much better agreement with measurements (Jonson and Travnikov, 2010). As the convective scheme is such a new addition to the EMEP model, and such schemes are more uncertain, we run here versions with and without the scheme (Stevenson et al., 2006).

Concerning emissions and chemical species, it should be noted that there is a large difference between CO and C_2H_6 in the model system. CO is a well-defined pollutant

ACPD
11, 13723–13767, 2011

with its own emission data bases. Such CO emissions data are thought to be fairly reliable over Europe and North America at least, although with larger uncertainties in other parts of the globe. On the other hand, C_2H_6 is a compound whose emissions are not explicitly mapped within the EMEP model. Instead, emissions of non-methane volatile organic compound (NMVOC) are available, distributed in 10 so-called SNAP sectors, with e.g. SNAP4 representing production processes, SNAP5 extraction and distribution of fossil-fuels, SNAP7 representing motor vehicles, etc. For each of these SNAP categories we have a default speciation profile, in which the percentage of C_2H_6 is specified. This profile is largely based upon emissions data from the UK however (Passant, 2002), and its validity in other areas is questionable. As C_2H_6 has very particular emission sources which will not be captured by such a simple percentage-contribution system, e.g. from gas-leakage, it is actually unlikely that the model's emission inventory for this compound is of sufficient quality to derive a meaningful trend analysis. Further, the model's C_2H_6 is actually a surrogate compound, representing not just real C_2H_6 but also some other low-reactivity compounds. For these reasons we will present the FTIR trends of CO and C_2H_6, but concentrate on the modeled trends of CO.

5 Method

The European-scale version of the EMEP model is first run over the time-period 1996-2006. These runs are intended to firstly evaluate the model's CO (and to a lesser extent) C_2H_6 fields, and secondly to determine the extent to which the changes in emissions and chemistry over the European domain can account for changes observed in the FTIR network. The global-scale EMEP model is essentially the same as the European-scale model, but not so dependent on initial and external boundary conditions, and driven by a different meteorological driver. As well as accounting for intercontinental transport, the global model is also able to account for recirculation of those air masses from Europe which pass beyond the boundaries of the European model. A comparison of the global model against FTIR measurements and the European model

ACPD
11, 13723–13767, 2011

is also performed. The global-scale model is then used in a series of sensitivity scenarios to investigate possible cause for the CO trends seen in the FTIR measurements. The model versions and sensitivity scenarios are summarized in Table 3.

5.1 Calculations of partial columns

Since both the European and global-scale EMEP model domains only extend up to 100 hPa, whereas the FTIR data extends throughout the whole atmosphere, partial columns from the FTIR measurements have to be derived for comparability. The partial columns consist of the tropospheric columns and those parts of the stratospheric columns that are below 100 hPa. These are simply calculated by subtracting the average part of the total columns above 100 hPa from the total columns. The averages are based on the retrieved FTIR profiles from Harestua and Jungfraujoch in the CO case and Harestua in the C_2H_6 case. The CO average is $6.1\pm2.2\times10^{16}$ molecules cm^{-2} and the C_2H_6 average is $5.0\pm2.2\times10^{14}$ molecules cm^{-2}, this corresponds to ~3-6 % and ~2 % of the total columns for each species, respectively. The uncertainties are presented on a 2-σ level. FTIR partial columns, in this case above 12 km, have earlier been reported to be at most 10 % and 7 % of the total column for CO and C_2H_6, respectively (Zhao et al., 2002).

The EMEP model data was obtained from discrete constant layers for both the European and global-scale models. To adjust the model to the actual altitude of the FTIR measurement stations, a linear interpolation, based on the difference between the station altitude and average topographical altitude in the grid area used by the EMEP model, was applied. Fagerli et al. (2007) discussed this issue in more detail, but for this exercise, the simple height-based interpolation is assumed to be sufficient for the model evaluation. The trend sensitivity study is not affected by the model baseline, i.e. the interpolation, since it is based on relative changes.

ACPD
11, 13723–13767, 2011

5.2 Trends and tracers

The FTIR trends are estimated with a method developed by Angelbratt et al. (2011). The method is based on multiple linear regressions where other data such as surface pressure and total column of hydrogen fluoride (HF) are used to reduce the variability in the FTIR time series and thereby explain part of the atmospheric dynamics resulting e.g. from tropopause changes or from the presence of the polar vortex. The model also contains a function that captures the seasonal fluctuations and the linear trend. Trends are estimated from the EMEP model by using simple linear regression. When estimating confidence intervals for the trends both of the above mentioned methods assume that the residuals (data minus trend model) are normal distributed, are free from auto-correlation and have equal variance around zero. The method of confidence interval on individual regression coefficients described in Montgomery et al. (2008) is used.

Tracers for CO and C_2H_6 have been introduced into the EMEP model, in order to track concentrations originating from the boundary and initial conditions (BICs). Tracers are lost to OH using the same rates as for CO and C_2H_6, but the tracers do not influence the chemical simulations. Thus, at the start of the simulation the modeled concentrations of CO and C_2H_6 are identical to their tracer counterparts. As the simulation proceeds emissions and chemical production and loss affect the real species, but the tracers respond only to advection and chemical loss. As the European-scale model has a limited spatial domain it can be heavily influenced by BICs, so that the tracer concentrations frequently amount to a large percentage of the real concentrations. The global-scale model is mainly influenced at the start of the simulation (see Sect. 6).

5.3 Sensitivity analysis for CO trends

To find possible causes for the estimated CO trends in the FTIR dataset, see Sect. 6.1.2, a series of sensitivity scenarios are tested in the global-scale model, the

ACPD
11, 13723–13767, 2011

scenarios are summarized in Table 3 and are described in detail below. As a base-simulation we use the standard model, with convection, but without forest fires (Gc) and all the sensitivity scenarios are compared with this simulation regarding the average value for 2006. The scenarios have been chosen to loosely represent known emission changes or climate effects and the mass balance are schematically described in Eq. (3), where P represent the production terms and D the destruction of CO in Tg yr^{-1}. In this paper, $P_{\text{Anthropogenic}}$ is defined as the CO emissions, mainly from combustion in industrial processes and the transport and energy sector while forest fires, savannah and agricultural waste burning is included in the $P_{\text{biomass burning}}$ term. The $P_{\text{CH4oxidation}}$ and $P_{\text{BVOC oxidation}}$ are defined as the formation of CO from the oxidation of these species with the OH radical. CO can also be formed in biological processes in soils and oceans and thus the $P_{\text{Biological}}$ term in Eq. (3). The main sink of CO is the reaction with the OH radical and thereby the destruction term D_{OH}.

$$\text{Trend} = P_{\text{Anthropogenic}} + P_{\text{Biomass burning}} + P_{\text{CH}_4\text{ oxidation}} + P_{\text{BVOC oxidation}} + P_{\text{Biological}} - D_{\text{OH}} \quad (3)$$

In the first two scenarios a reduction of anthropogenic CO emissions by 20 % in Europe and North American are tested (GcEUR20 and GcNA20) and this corresponds to a ∼2 % decrease per year during the 11 year period of 1996–2006 for which the FTIR measurements are taken. In Monks et al. (2009) and the EDGAR database v. 4.0 (2009) the anthropogenic CO emissions in Europe have shown to decrease by 1.7 % yr^{-1} to 4.5 % yr^{-1} and the North American emissions have show to decrease by 2.1 % yr^{-1} to 3.7 % yr^{-1}, where the trends are based on data from the late 1990s and early 2000. The reported emission reductions for both continents indicate that our reduction of 2 % yr^{-1} is a reasonable value to use in the two sensitivity scenarios. Further, we have decided to use a reduction in the lower range for both of the scenarios not to overestimate the change in the modeled CO partial columns.

Unlike North America and Europe, many counties in Asia have increased their CO emissions during the last decades. In the third scenario (GcEA20) we investigate how a 20 % increase in the East Asian anthropogenic CO emissions is affecting the CO trends

ACPD
11, 13723–13767, 2011

seen in Europe. We define East Asia as China and Japan, and for model simulations use the same area as defined by Fiore et al. (2009). According to Monks et al. (2009), China has increased its CO emissions by approximately 15 % from 1996 to 2003 where the years after 2000 shows the strongest increase. Data from the EDGAR emission database v.4.0 (EDGAR, 2009) show a 24 % increase for China and a 4 % decrease for Japan from the 1996 to 2005 time period. The reported emission data from China and Japan indicate that a 20 % increase during the 1996-2006 period is a reasonable assumption.

In scenarios four and five, GcEurAll20 and GcNAAll20, the emissions from all anthropogenic sources (CO, NO_x, NMVOC, SO_x, and NH_3) are reduced with 20 % for Europe and North America (again using the Fiore et al. (2009) domain definitions). Since both CO and the other species have decreased these scenarios illustrate more realistic situations where the chemical interactions between the species are included in the simulation. Scenario six corresponds to a 20 % increase for the same species as in four and five but for East Asia (GcEAAll20).

In scenario seven the global surface temperature as used in the BVOC calculations are increased by 0.2 °C (GcT0.2). According to Hansen et al. (2006) the global temperature has increased with 0.2 °C yr^{-1} the last decades and since the BVOC emissions are strongly temperature dependent, such emissions should also have increased.

In the last sensitivity scenario ($GcCH_4$1.2) it is investigated how the partial columns of CO are affected by the methane (CH_4) concentrations. Both surface concentration and total column measurements of CH_4 have shown to increase from 1996 to 1999 and thereafter flatten out towards a zero trend for the rest of the studied period (Dlugokencky et al., 2009) (Angelbratt et al., 2011). The average increase over the first three years was 0.4 % yr^{-1}. A proper modeling assessment of these CH_4 changes would need to run over many years because of the lifetime of CH_4 (~10 years) (Fiore et al., 2009). Here we make a first order approximation and calculated the effect of a single 1.2 % yr^{-1} emission change calculated over one year (2006).

ACPD
11, 13723–13767, 2011

5.4 Uncertainty analysis

A number of other tests have been conducted with the global model which explores the importance of some model assumptions. As noted in the introduction, the convection routine is new to the EMEP model and optional. Although convection is unquestionably important to atmospheric transport, the parameterization of this in models is also quite uncertain (Stevenson et al., 2006). For this reason we have run a model version (G, Table 3) without convection. A second test with the global model is the introduction of forest-fire emissions. Although such emissions should in principal be part of a default model run, we only have 8-day average emissions. Thus, when comparing with daily FTIR data, we have chosen to omit these data from the base-case but in test Gcff, forest-fire emissions are added for comparison. As discussed in section 5.1 (and Fagerli et al., 2007), model results are derived as an interpolation between discrete model layers, and some uncertainty is associated with this procedure. Two tests (Gc-high, Gc-low, Table 3) are conducted in which the model results are taken from model-layers higher than, or lower than, than this default. Also the uncertainty in the derived partial columns, Sect. 5.1, is investigated in two tests, FTIR-high and FTIR-low. Finally, we have conducted one more, extreme, test of the BVOC emissions, namely setting all such emissions to zero (Gcnobvoc). This test is designed purely to explore the magnitude of CO associated with BVOC emissions. Such emissions are in fact one of the most uncertain inputs to the CTMs, at least over North America and Europe where other emissions are known with reasonable accuracy, and according to Granier et al. (2000), BVOC contribute to up to 18 % of the global budget of CO. Simpson et al. (1999) estimated a factor 2–3 uncertainty for European isoprene emissions (and much worse for other BVOC), and Warneck (2000) found factor of two differences between two BVOC inventories in the United States, with measurement-based data unable to distinguish which was best.

ACPD
11, 13723–13767, 2011

6 Results and discussion

6.1 European model 1996–2006

6.1.1 Average partial column and seasonal amplitude

The comparison of the European-scale model with the CO and C_2H_6 FTIR measurements is presented in Figs. 1 and 2, respectively. In general, strong similarities between the model and measurements can be seen for both species. To further quantify the differences; average values, standard deviations and seasonal amplitudes are calculated for the two species, these are presented in Table 4. Compared to the low-level sites, the Alpine stations have a lower average partial column and seasonal amplitude due to their high altitude and thereby the fact that a large part of the partial column is located below the station.

As noted in Sect. 4, the European-scale model uses climatological (monthly) boundary and initial conditions (BICs) for CO and C_2H_6, and these values strongly determine the model's concentrations, and hence are responsible for much of the good agreement. The BIC influence is quantified by tracers and those are presented in Table 5 where it can be seen that columns at the modeled stations close to the model boundary are dominated by the BICs, while columns at the stations further away from the boundary include more information generated within the model. It can also be seen that more information is from the BICs for C_2H_6 than for CO.

A clear difference in CO between the model and the measurements can be seen in the year 1998 and 2002/2003 for most of the stations and this is particularly visible at Jungfraujoch and Kiruna in 1998. For C_2H_6 these differences are not so clear although they can be seen for example at Jungfraujoch and Kiruna in 1998. During these two time periods, large scale forest fires were present in North America and Russia and the CO contributions to the atmosphere were captured by the FTIR measurements (Yurganov et al., 2004, 2005). As noted in Sect. 4, forest fire emissions were not available at consistent time-resolution over the 11 years of this study, and so omitted

ACPD
11, 13723–13767, 2011

from the European-scale calculations. Further, and probably most importantly, the model domain does not include North America and non-European parts of Russia and is hence highly dependent on the lateral boundary conditions.

Compared to the measurements, the model shows a slight phase shift for all the participating stations regarding CO and C_2H_6. For CO the model tends to overestimate the seasonal amplitude and underestimate the average partial column For C_2H_6 on the other hand, the model overestimates both the average partial column and seasonal amplitude and deviates sometimes with as much as a factor of two. For both species, the model captures the inter station variability quite well for both the average partial columns and the seasonal amplitudes. Although C_2H_6 has much less importance for EMEP modeling purposes (usually aimed at boundary layer ozone, or acidification and health issues) than CO, these results suggest a need to modify the global boundary conditions for the European EMEP model, and to re-evaluate the emission inventories for this compound.

6.1.2 Trends

All FTIR stations show significant negative CO trends on the 2-σ level, this is presented in Table 6. For the 1996 to 2006 time period, Harestua and Kiruna are in close agreement to each other while the trends at Jungfraujoch and Zugspitze deviate more than expected, given their close geographical and altitude location. Compared to Jungfraujoch, Zugspitze has very few measurements in 1996 and 1997; this together with the unusually high values in 1998 and 1999 is probably one of the reasons to the strong negative trend at Zugspitze. The explanation is strengthened by the estimated trends from the 1998 to 2006 time period, where the trends are in much closer agreement for the two stations. Earlier, Zhao et al. (2002) have reported CO trends for the time period 1995–2000 of $-2.1\pm0.2\,\%\,yr^{-1}$ from FTIR tropospheric columns measured at two Japanese stations. Novelli et al. (2003) have reported an average trend from 1991–2001 for the Northern Hemisphere, from a network of flask sample measurements, of $-0.92\pm0.15\,\%\,yr^{-1}$. Gardiner et al. (2008) have reported insignificant FTIR total col-

ACPD
11, 13723–13767, 2011

umn trends for Europe of -0.1±0.46 % yr^{-1} to −0.58±0.69 % yr^{-1}, this based on data from 1995–2004. Gilge et al. (2010) have reported in-situ trends for the time period of 1996-2007 for Jungfraujoch and 1995-2002 for Zugspitze of roughly −2.1±0.7 % yr^{-1}. The earlier reported trends and the ones presented in this paper indicate the presence of a negative trend in the Northern Hemisphere, although with a magnitude depending on the geographical location of the measurement station, the covered time period and the type of measurement.

Significant negative C_2H_6 trends are estimated for all FTIR stations, see Table 6. The trends are stronger compared to those of CO and vary from −2.25±0.35 % yr^{-1} to −1.09±0.25 % yr^{-1}. Again Harestua and Kiruna are in close agreement and Jungfraujoch and Zugspitze differ despite their proximity. To the author's knowledge, very few trend estimations have been performed for C_2H_6. Except the trends given in Rinsland et al. (1998) and Mahieu et al. (1997), the trends in this paper could be compared with the solar FTIR trends from 1995 to 2004 of: −0.63±0.37 % yr^{-1} from Kiruna, −0.65±0.32 % yr^{-1} for Harestua, −1.14±0.60 % yr^{-1} for Zugspitze and −1.05±0.35 % yr^{-1} for Jungfraujoch, presented by Gardiner et al. (2008).

No significant trends for CO and C_2H_6 have been found in the European-scale EMEP model. Since the model boundary conditions do not contain any trend components and most of the information at each station comes from the boundary conditions, see Table 5, we conclude that the model domain is too small for detection trends from species with a lifetime as long as two months. To model a more realistic alternative regarding CO trends the global-scale model will be used in Sect. 6.2.2.

6.2 Global model 2006

6.2.1 Evaluation of global-scale model

The comparison of the global and European-scale model with the FTIR measurements for year 2006 is presented in Fig. 3 and Figure 4 for CO and C_2H_6, respectively. The average values for each station and species is also presented in Table 7.

ACPD
11, 13723–13767, 2011

The global-scale model reproduces the FTIR data slightly better than the European model for the partial columns of CO at all participating stations. The biggest difference is at the stations located at higher latitudes where the European model tends to overestimates the partial columns while the global model is in good agreement with the measurements. The overestimation by the European model at high latitudes is probably due to the high influence from the boundary conditions at these locations. Both the global and European model have problems reproducing the partial columns of C_2H_6. The global model significantly underestimates the partial columns at all stations and for some with as much as a factor of two. Also the European model underestimates the partial column but not as much as the global model.

6.2.2 Sensitivity of CO trends

The outcome of the global-scale model sensitivity scenarios for CO is presented in Table 8 as relative change in the CO partial column per year. The trends are calculated as the relative difference in the 2006 average value for each scenario, relative to the base scenario, excluding the January and February months due to their high influence of the model start conditions.

The European anthropogenic CO reduction with 20 % (GcEUR20) has the largest impact on the modeled partial columns of all scenarios and could by itself account for a negative trend of 0.47-0.83 % yr^{-1}. Also, a 20 % reduction in the North American anthropogenic CO emissions (GcNA20) causes negative trends in the modeled partial column from 0.20–0.22 % yr^{-1}. The increase in the East Asian anthropogenic CO emission with 20 % (GcEA20) gives a positive contribution to the modeled European partial column trends of 0.15–0.18 % yr^{-1}, this region has a slightly smaller impact on the absolute European trends than North America. A global increase in the CH_4 column by 0.4 % yr^{-1} ($GcCH_4$1.2) and an increase in the global temperature by 0.2 °C during the 11 years period give a positive contribution to the modeled trends of ~0.15 % yr^{-1} for all stations. Although the two scenarios are rough estimations this highlights the fact that

ACPD
11, 13723–13767, 2011

CO seems to be sensitive to both the global temperature and the CH_4 concentration.

When adding the five sensitivity scenarios discussed above (shown as ΣGc in Table 8), Jungfraujoch, Harestua and Kiruna will have modeled trends that are close to the measured ones while the modeled trend at Zugspitze deviate with a factor of two from the measured one. The modeled trends follow the measured trends with a smaller trend at Jungfraujoch and larger trends at Harstua and Kiruna. It can also be seen that the modeled trend at Zugspitze is larger than the one for Jungfraujoch. To exclude the altitude difference between the stations as a reason for this behavior, the trends at the ground layer are also modeled, this is presented in Table 9. In the comparison it can be seen that the trend difference is 0.07 % yr^{-1} at the ground layer while it is 0.10 % yr^{-1} when adjusting for the station levels. From this we conclude that the modeled trend difference between Jungfraujoch and Zugspitze is not due to the different altitudes of the stations but rather has to do with the origin of the air masses at each station. This fact might also be an additional explanation to the measured trend difference between Jungfraujoch and Zugspitze, presented in Sect. 6.1.2. The modeled trends at Bremen and Ny-Ålesund stands out a bit compared to the other stations. The small trend at Ny-Ålesund is not surprising since the station is located in the far north and is hence less affected by the European CO reduction. Bremen on the other has a central location and is affected by European CO reductions for all wind directions.

The 20 % reduction and increase in emissions of all anthropogenic species (GcEURAll20, GcNAAll20, GcEAAll20) represents the change in OH chemistry that occur due to a change in the NO_x, NH_3, NMVOC and SO_x concentrations and thereby the assumed change in the CO partial columns. It was shown that the difference between the Gc20 and Gc20All scenarios hardly differs at all between the model calculations for the three regions. Since OH affect the CO concentrations both as (1) a sink and (2) a source through the oxidation of VOCs and CH_4 it turns out that these two processes cancel out each other and that the modeled CO partial columns are almost insensitive to changes in NO_x, NH_3, NMVOC and SO_x.

ACPD
11, 13723–13767, 2011

When considering the mass balance for CO in Eq. (3) we have investigated the presence of trends in three sources namely, anthropogenic CO emissions, oxidation of CH_4 and BVOC (through the GcT0.2 scenario) while possible trends in biomass burning and in the OH radical concentration due to factors other than the emission changes explored above have not been taken into account. Both the OH radical and biomass burning have large inter-annual fluctuations, this is for example shown by Yurganov et al. (2004, 2005) and Montzka et al. (2011), and these fluctuations contributes to the uncertainties in the estimated FTIR trends. To outline the effect on the CO trends of possible changes in the OH radical and biomass burning further studies are needed.

6.2.3 Uncertainty analysis

As discussed in Sect. 5.4, we have conducted a number of tests designed to quantify some of the uncertainties in the calculations, concerning convection, forest-fires and BVOC emissions but also uncertainties related to the derivation of partial columns from the FTIR measurements and the interpolation between the model layers. In Fig. 5 the results of these tests are illustrated for Harestua. It can be seen that the model with the forest fire module (Gcff) in general reproduce the FTIR measurements best compared to the other two versions (G and Gc) where G is close to Gcff while Gc is underestimating the measurements. This illustrate that the convection module decrease the estimated partial columns while the forest fire module increases the partial columns and that the two modules together almost cancel out each other. It is also shown that the derivation of the partial columns from the measurements is almost insensitive to the seasonal variation of the 100 hPa level, this is not unexpected since a very small fraction of the partial column is located around this level. The model is more sensitive to the interpolation between the layers and the BVOC emissions and when removing all North American BVOC emission a large underestimation of the partial columns of CO is seen.

ACPD
11, 13723–13767, 2011

7 Conclusions

In this paper we have shown negative linear trends from partial columns of CO and C_2H_6 measured with the ground based solar FTIR technique at four European stations, Jungfraujoch, Zugspitze, Harestua and Kiruna. To outline possible reasons for the measured negative CO trends the global-scale EMEP model was used in a series of sensitivity scenarios. It was found that the reduction in the European anthropogenic CO emissions, during the 1996–2006 period, to a large extent could explain the negative trends measured at the FTIR stations. Also, the decrease in North American and increase in East Asian anthropogenic CO emissions affected the measured CO partial columns in Europe. This paper should be considered as a first attempt to explain the CO trends seen in the FTIR measurements. Since the global-scale EMEP model only was working for year 2006 the analysis can be improved when the model is available for the whole time period (1996-2006). Furthermore, of great interest is the effects of the variations in the OH radical and biomass burning on the trends in CO. This has been outside the scope of this article and a more detailed analysis, on a statistical basis, is needed to quantify the exact reasons for the measured trends.

Acknowledgements. The authors would like to thank the EU projects UFTIR and HYMN and the Swedish Environmental Protection Agency for financial support. Further, Anders Strandberg, Elisabeth Unden and Glenn Persson are thanked for measurement and data retrieval support. University of Liège was supported by the Belgian Science Policy Office (PRODEX and SSD programs) as well as by the European Union projects mentioned here above. We are grateful to the many colleagues who contributed to the FTIR data acquisition at the Jungfraujoch and would like to thank the International Foundation High Altitude Research Stations Jungfraujoch and Gornergrat (HFSJG, Bern) for supporting the facilities needed to perform the observations. The work of David Simpson was further supported by the EU 6th Framework Programme EU-CAARI project (contract 036833-2), as well as by Cooperative Programme for Monitoring and Evaluation of the Long-Range Transmission of Air Pollutants in Europe (EMEP) under UNECE.

ACPD
11, 13723–13767, 2011

References

Aikin, A. C., Herman, J. R., Maier, E. J., and Mcquillan, C. J.: Atmospheric Chemistry of Ethane and Ethylene, J. Geophys. Res.-Ocean. Atmos., 87, 3105–3118, 1982.

Andersson-Skold, Y. and Simpson, D.: Comparison of the chemical schemes of the EMEP MSC-W and IVL photochemical trajectory models, Atmos. Environ., 33, 1111–1129, 1999.

Angelbratt, J., Mellqvist, J., Blumenstock, T., Borsdorf, T., Brohede, S., Duchatlet, P., Forster, F., Hase, F., Mahieu, E., Murtagh, D., Petersen, K., Schneider, M., Sussmann, R., and Urban, J.: A new method to detect long term trends of methane (CH_4) and nitrous oxide (N_2O) total columns measured within the NDACC ground-based high resolution solar FTIR network, Atmos. Chem. Phys. Discuss., 11, 8207–8247, doi:10.5194/acpd-11-1-2010, 2011.

Berge, E., and Jakobsen, H. A.: A regional scale multi-layer model for the calculation of long-term transport and deposition of air pollution in Europe, Tellus B-Chem. Phys. Meteorol., 50, 205–223, 1998.

Blake, D. R. and Rowland, F. S.: Global Atmospheric Concentrations and Source Strength of Ethane, Nature, 321, 231–233, 1986.

Crutzen, P. J., Lawrence, M. G., and Pöschl, U.: On the background photochemistry of tropospheric ozone, Tellus a – Dynam. Meteorol. Oceanogr., 51, 123–146, 1999.

DeMazière, M., Vigouroux, C., Gardiner, T., Coleman, M., Woods, P., Ellingsen, K., Gauss, M., Isaksen, I., Blumenstock, T., Hase, F., Kramer, I., Camy-peyret, C., Chelin, P., Mahieu, E., Demoulin, P., Duchatelet, P., Mellqvist, J., Strandberg, A., Velazco, V., Notholt, J., Sussmann, R., Stremme, W., and Rockmann, A.: The exploitation of ground-based Fourier transform infrared observations for the evaluation of tropospheric trends of greenhouse gases over Europe, Environ. Sci., 2, 283–293, 2005.

Derwent, R., Simmonds, P., Seuring, S., and Dimmer, C.: Observations and interpretation of the seasonal cycles in the surface concentrations of ozone and carbon monoxide at Mace Head, Ireland from 1990 to 1994, Atmos. Environ., 32, 145–157, 1998.

Dlugokencky, E. J., Bruhwiler, L., White, J. W. C., Emmons, L. K., Novelli, P. C., Montzka, S. A., Masarie, K. A., Lang, P. M., Crotwell, A. M., Miller, J. B., and Gatti, L. V.: Observational constraints on recent increases in the atmospheric CH_4 burden, Geophys. Res. Lett., 36, L18803, doi:10.1029/2009gl039780, 2009.

Duchatelet, P., Demoulin, P., Hase, F., Ruhnke, R., Feng, W., Chipperfield, M. P., Bernath, P. F., Boone, C. D., Walker, K. A., and Mahieu, E.: Hydrogen fluoride total and partial column time

ACPD
11, 13723–13767, 2011

series above the Jungfraujoch from long-term FTIR measurements: Impact of the line-shape model, characterization of the error budget and seasonal cycle, and comparison with satellite and model data, J. Geophys. Res.-Atmos., 115, D22306, doi:10.1029/2010jd014677, 2010.

EDGAR: European Commission, Joint Research Centre (JRC)/Netherlands Environmental Assessment Agency (PBL). Emission Database for Global Atmospheric Research (EDGAR), release version 4.0., available online at: http://edgar.jrc.ec.europa.eu, 2009.

Ehhalt, D. H., Schmidt, U., Zander, R., Demoulin, P., and Rinsland, C.: Seasonal cycle and secular trend of the total and tropospheric column abundance of ethane above the Jungfraujoch, J. Geophys. Res., 96, 4985–4994, 1991.

Emmons, L. K., Hauglustaine, D. A., Müller, J.-F., Carroll, M. A., Brasseur, G. P., Brunner, D., Staehelin, J., Thouret, V., and Marenco, A.: Data composites of airborne observations of tropospheric ozone and its precursors, J. Geophys. Res., 105, 20497–20538, 2000.

Fagerli, H. and Aas, W.: Trends of nitrogen in air and precipitation: Model results and observations at EMEP sites in Europe, 1980-2003, Environ. Pollut., 154, 448–461, doi:10.1016/j.envpol.2008.01.024, 2008.

Fagerli, H., Legrand, M., Preunkert, S., Vestreng, V., Simpson, D., and Cerqueira, M.: Modeling historical long-term trends of sulfate, ammonium, and elemental carbon over Europe: A comparison with ice core records in the Alps, J. Geophys. Res.-Atmos., 112, D23S13, doi:10.1029/2006jd008044, 2007.

Finlayson-Pitts, B. J. and Pitts, J. N.: Chemistry of the upper and lower atmosphere : theory, experiments, and applications, Academic Press, San Diego,USA, 22, 969 pp., 2000.

Fiore, A. M., Dentener, F. J., Wild, O., Cuvelier, C., Schultz, M. G., Hess, P., Textor, C., Schulz, M., Doherty, R. M., Horowitz, L. W., MacKenzie, I. A., Sanderson, M. G., Shindell, D. T., Stevenson, D. S., Szopa, S., Van Dingenen, R., Zeng, G., Atherton, C., Bergmann, D., Bey, I., Carmichael, G., Collins, W. J., Duncan, B. N., Faluvegi, G., Folberth, G., Gauss, M., Gong, S., Hauglustaine, D., Holloway, T., Isaksen, I. S. A., Jacob, D. J., Jonson, J. E., Kaminski, J. W., Keating, T. J., Lupu, A., Marmer, E., Montanaro, V., Park, R. J., Pitari, G., Pringle, K. J., Pyle, J. A., Schroeder, S., Vivanco, M. G., Wind, P., Wojcik, G., Wu, S., and Zuber, A.: Multimodel estimates of intercontinental source-receptor relationships for ozone pollution, J. Geophys. Res.-Atmos., 114, D04301, doi:10.1029/2008jd010816, 2009.

Gardiner, T., Forbes, A., de Mazière, M., Vigouroux, C., Mahieu, E., Demoulin, P., Velazco, V., Notholt, J., Blumenstock, T., Hase, F., Kramer, I., Sussmann, R., Stremme, W., Mellqvist, J., Strandberg, A., Ellingsen, K., and Gauss, M.: Trend analysis of greenhouse gases over

ACPD
11, 13723–13767, 2011

Europe measured by a network of ground-based remote FTIR instruments, Atmos. Chem. Phys., 8, 6719–6727, doi:10.5194/acp-8-6719-2008, 2008.
Gilge, S., Plass-Duelmer, C., Fricke, W., Kaiser, A., Ries, L., Buchmann, B., and Steinbacher, M.: Ozone, carbon monoxide and nitrogen oxides time series at four alpine GAW mountain stations in central Europe, Atmos. Chem. Phys., 10, 12295–12316, doi:10.5194/acp-10-12295-2010, 2010.
Granier, C., Petron, G., Muller, J. F., and Brasseur, G.: The impact of natural and anthropogenic hydrocarbons on the tropospheric budget of carbon monoxide, Atmos. Environ., 34, 5255–5270, 2000.
Guenther, A. B., Zimmerman, P. R., Harley, P. C., Monson, R. K., and Fall, R.: Isoprene and Monoterpene Emission Rate Variability – Model Evaluations and Sensitivity Analyses, J. Geophys. Res.-Atmos., 98, 12609–12617, 1993.
Hansen, J., Sato, M., Ruedy, R., Lo, K., Lea, D. W., and Medina-Elizade, M.: Global temperature change, P. Natl. Acad. Sci. USA, 103, 14288–14293, doi:10.1073/pnas.0606291103, 2006.
Hase, F., Blumenstock, T., and Paton-Walsh, C.: Analysis of the instrumental line shape of high-resolution Fourier transform IR spectrometers with gas cell measurements and new retrieval software, Appl. Optics, 38, 3417–3422, 1999.
Hase, F., Hannigan, J. W., Coffey, M. T., Goldman, A., Hopfner, M., Jones, N. B., Rinsland, C. P., and Wood, S. W.: Intercomparison of retrieval codes used for the analysis of high-resolution, ground-based FTIR measurements, J. Quant. Spectrosc. Radiat. Trans., 87, 25–52, doi:10.1016/j.jqsrt.2003.12.008, 2004.
Holloway, T., Levy, H., and Kasibhatla, P.: Global distribution of carbon monoxide, J. Geophys. Res.-Atmos., 105, 12123–12147, 2000.
HTAP, T.: Hemispheric Transport of air pollution 2007 Economic commision for Europe, Geneva, Air Pollution Studies No. 16, United Nations, New York and Geneva, 2007.
Isaksen, I. S. A., Granier, C., Myhre, G., Berntsen, T. K., Dalsoren, S. B., Gauss, M., Klimont, Z., Benestad, R., Bousquet, P., Collins, W., Cox, T., Eyring, V., Fowler, D., Fuzzi, S., Jockel, P., Laj, P., Lohmann, U., Maione, M., Monks, P., Prevot, A. S. H., Raes, F., Richter, A., Rognerud, B., Schulz, M., Shindell, D., Stevenson, D. S., Storelvmo, T., Wang, W. C., van Weele, M., Wild, M., and Wuebbles, D.: Atmospheric composition change: Climate-Chemistry interactions, Atmos. Environ., 43, 5138–5192, doi:10.1016/j.atmosenv.2009.08.003, 2009.
Jonson, J. E., Simpson, D., Fagerli, H., and Solberg, S.: Can we explain the trends in European

ACPD
11, 13723–13767, 2011

ozone levels?, Atmos. Chem. Phys., 6, 51–66, doi:10.5194/acp-6-51-2006, 2006.
Jonson, J. E., Stohl, A., Fiore, A. M., Hess, P., Szopa, S., Wild, O., Zeng, G., Dentener, F. J., Lupu, A., Schultz, M. G., Duncan, B. N., Sudo, K., Wind, P., Schulz, M., Marmer, E., Cuvelier, C., Keating, T., Zuber, A., Valdebenito, A., Dorokhov, V., De Backer, H., Davies, J., Chen, G. H., Johnson, B., Tarasick, D. W., Stubi, R., Newchurch, M. J., von der Gathen, P., Steinbrecht, W., and Claude, H.: A multi-model analysis of vertical ozone profiles, Atmos. Chem. Phys., 10, 5759–5783, doi:10.5194/acp-10-5759-2010, 2010.
Khalil, M. A. K. and Rasmussen, R. A.: Carbon-Monoxide in the Earths Atmosphere – Indications of a Global Increase, Nature, 332, 242–245, 1988.
Khalil, M. A. K. and Rasmussen, R. A.: Global Decrease in Atmospheric Carbon-Monoxide Concentration, Nature, 370, 639–641, 1994.
Lelieveld, J., Peters, W., Dentener, F. J., and Krol, M. C.: Stability of tropospheric hydroxyl chemistry, J. Geophys. Res.-Atmos., 107, 4715, doi:10.1029/2002jd002272, 2002.
Logan, J. A.: An analysis of ozonesonde data for the troposphere: Recommendations for testing 3-D models and development of a gridded climatology for tropospheric ozone, J. Geophys. Res.-Atmos., 104, 16115–16149, 1999.
Mahieu, E., Zander, R., Delbouille, L., Demoulin, P., Roland, G., and Servais, C.: Observed trends in total vertical column abundances of atmospheric gases from IR solar spectra recorded at the Jungfraujoch, J. Atmos. Chem., 28, 227–243, 1997.
Metzger, S., Dentener, F., Pandis, S., and Lelieveld, J.: Gas/aerosol partitioning: 1. A computationally efficient model, J. Geophys. Res.-Atmos., 107, 4312, doi:10.1029/2001jd001102, 2002.
Monks, P. S., Granier, C., Fuzzi, S., Stohl, A., Williams, M. L., Akimoto, H., Amann, M., Baklanov, A., Baltensperger, U., Bey, I., Blake, N., Blake, R. S., Carslaw, K., Cooper, O. R., Dentener, F., Fowler, D., Fragkou, E., Frost, G. J., Generoso, S., Ginoux, P., Grewe, V., Guenther, A., Hansson, H. C., Henne, S., Hjorth, J., Hofzumahaus, A., Huntrieser, H., Isaksen, I. S. A., Jenkin, M. E., Kaiser, J., Kanakidou, M., Klimont, Z., Kulmala, M., Laj, P., Lawrence, M. G., Lee, J. D., Liousse, C., Maione, M., McFiggans, G., Metzger, A., Mieville, A., Moussiopoulos, N., Orlando, J. J., O'Dowd, C. D., Palmer, P. I., Parrish, D. D., Petzold, A., Platt, U., Poschl, U., Prevot, A. S. H., Reeves, C. E., Reimann, S., Rudich, Y., Sellegri, K., Steinbrecher, R., Simpson, D., ten Brink, H., Theloke, J., van der Werf, G. R., Vautard, R., Vestreng, V., Vlachokostas, C., and von Glasow, R.: Atmospheric composition change – global and regional air quality, Atmos. Environ., 43, 5268–5350, doi:10.1016/j.atmosenv.2009.08.021, 2009.

ACPD
11, 13723–13767, 2011

Montgomery, D. C., Jennings, C. L., and Kulahci, M.: Introduction to time series analysis and forecasting, Wiley series in probability and statistics, Wiley-Interscience, Hoboken, NJ, USA, 11, 445 pp., 2008.

Montzka, S. A., Krol, M., Dlugokencky, E., Hall, B., Jockel, P., and Lelieveld, J.: Small Interannual Variability of Global Atmospheric Hydroxyl, Science, 331, 67–69, doi:10.1126/science.1197640, 2011.

Novelli, P. C., Masarie, K. A., Lang, P. M., Hall, B. D., Myers, R. C., and Elkins, J. W.: Reanalysis of tropospheric CO trends: Effects of the 1997–1998 wildfires, J. Geophys. Res.-Atmos., 108, 4464, doi:10.1029/2002jd003031, 2003.

Passant, N. R.: Speciation of UK emissions of non-methane volatile organic compounds, AEAT/ENV/R/0545 Issue 1, 2002.

Reidmiller, D. R., Fiore, A. M., Jaffe, D. A., Bergmann, D., Cuvelier, C., Dentener, F. J., Duncan, B. N., Folberth, G., Gauss, M., Gong, S., Hess, P., Jonson, J. E., Keating, T., Lupu, A., Marmer, E., Park, R., Schultz, M. G., Shindell, D. T., Szopa, S., Vivanco, M. G., Wild, O., and Zuber, A.: The influence of foreign vs. North American emissions on surface ozone in the US, Atmos. Chem. Phys., 9, 5027–5042, doi:10.5194/acp-9-5027-2009, 2009.

Rinsland, C. P., Jones, N. B., Connor, B. J., Logan, J. A., Pougatchev, N. S., Goldman, A., Murcray, F. J., Stephen, T. M., Pine, A. S., Zander, R., Mahieu, E., and Demoulin, P.: Northern and southern hemisphere ground-based infrared spectroscopic measurements of tropospheric carbon monoxide and ethane, J. Geophys. Res.-Atmos., 103, 28197–28217, 1998.

Rodgers, C. D.: Inverse Methods for Atmospheric Sounding, Series on Atmospheric, Ocean. Planet. Phys., 2, 55–63, 2000.

Sanderson, M. G., Dentener, F. J., Fiore, A. M., Cuvelier, C., Keating, T. J., Zuber, A., Atherton, C. S., Bergmann, D. J., Diehl, T., Doherty, R. M., Duncan, B. N., Hess, P., Horowitz, L. W., Jacob, D. J., Jonson, J. E., Kaminski, J. W., Lupu, A., MacKenzie, I. A., Mancini, E., Marmer, E., Park, R., Pitari, G., Prather, M. J., Pringle, K. J., Schroeder, S., Schultz, M. G., Shindell, D. T., Szopa, S., Wild, O., and Wind, P.: A multi-model study of the hemispheric transport and deposition of oxidised nitrogen, Geophys. Res. Lett., 35, L17815 doi:10.1029/2008gl035389, 2008.

Shindell, D. T., Faluvegi, G., Stevenson, D. S., Krol, M. C., Emmons, L. K., Lamarque, J. F., Petron, G., Dentener, F. J., Ellingsen, K., Schultz, M. G., Wild, O., Amann, M., Atherton, C. S., Bergmann, D. J., Bey, I., Butler, T., Cofala, J., Collins, W. J., Derwent, R. G., Doherty, R. M., Drevet, J., Eskes, H. J., Fiore, A. M., Gauss, M., Hauglustaine, D. A., Horowitz, L. W.,

ACPD
11, 13723–13767, 2011

Isaksen, I. S. A., Lawrence, M. G., Montanaro, V., Muller, J. F., Pitari, G., Prather, M. J., Pyle, J. A., Rast, S., Rodriguez, J. M., Sanderson, M. G., Savage, N. H., Strahan, S. E., Sudo, K., Szopa, S., Unger, N., van Noije, T. P. C., and Zeng, G.: Multimodel simulations of carbon monoxide: Comparison with observations and projected near-future changes, J. Geophys. Res.-Atmos., 111, D19306, doi:10.1029/2006jd007100, 2006.

Shindell, D. T., Chin, M., Dentener, F., Doherty, R. M., Faluvegi, G., Fiore, A. M., Hess, P., Koch, D. M., MacKenzie, I. A., Sanderson, M. G., Schultz, M. G., Schulz, M., Stevenson, D. S., Teich, H., Textor, C., Wild, O., Bergmann, D. J., Bey, I., Bian, H., Cuvelier, C., Duncan, B. N., Folberth, G., Horowitz, L. W., Jonson, J., Kaminski, J. W., Marmer, E., Park, R., Pringle, K. J., Schroeder, S., Szopa, S., Takemura, T., Zeng, G., Keating, T. J., and Zuber, A.: A multi-model assessment of pollution transport to the Arctic, Atmos. Chem. Phys., 8, 5353–5372, doi:10.5194/acp-8-5353-2008, 2008.

Simpson, D., Guenther, A., Hewitt, C. N., and Steinbrecher, R.: Biogenic Emissions in Europe .1. Estimates and Uncertainties, J. Geophys. Res.-Atmos., 100, 22875–22890, 1995.

Simpson, D., Winiwarter, W., Borjesson, G., Cinderby, S., Ferreiro, A., Guenther, A., Hewitt, C. N., Janson, R., Khalil, M. A. K., Owen, S., Pierce, T. E., Puxbaum, H., Shearer, M., Skiba, U., Steinbrecher, R., Tarrason, L., and Oquist, M. G.: Inventorying emissions from nature in Europe, J. Geophys. Res.-Atmos., 104, 8113–8152, 1999.

Simpson, D., Fagerli, H., Jonson, J., Tsyro, S., Wind, P., and Tuovinen, J.-P.: The EMEP Unified Eulerian Model. Model Description The Norwegian Meteorological Institute, Oslo, Norway, 2003a.

Simpson, D., Fagerli, H., Solberg, S., and Aas, W.: Photo-oxidants, EMEP MSC-W Report 1/2003, Part II, Unified EMEP Model performance. Norwegian Meteorological Institute, Oslo, Norway, 1/2003, Part II, 2003b.

Simpson, D., Tuovinen, J. P., Emberson, L., and Ashmore, M. R.: Characteristics of an ozone deposition module II: Sensitivity analysis, Water Air Soil Pollut., 143, 123–137, 2003c.

Simpson, D., Fagerli, H., Hellsten, S., Knulst, J. C., and Westling, O.: Comparison of modelled and monitored deposition fluxes of sulphur and nitrogen to ICP-forest sites in Europe, Biogeosciences, 3, 337–355, doi:10.5194/bg-3-337-2006, 2006.

Simpson, D., Michael Gauss, S. T., and Valdebenito, A.: Model Updates Transboundary acidification, eutrophication and ground level ozone in Europe EMEP Status Report 1/2010,, The Norwegian Meteorological Institute, Oslo, Norway, 2010.

Stevenson, D. S., Dentener, F. J., Schultz, M. G., Ellingsen, K., van Noije, T. P. C., Wild, O.,

ACPD
11, 13723–13767, 2011

Zeng, G., Amann, M., Atherton, C. S., Bell, N., Bergmann, D. J., Bey, I., Butler, T., Cofala, J., Collins, W. J., Derwent, R. G., Doherty, R. M., Drevet, J., Eskes, H. J., Fiore, A. M., Gauss, M., Hauglustaine, D. A., Horowitz, L. W., Isaksen, I. S. A., Krol, M. C., Lamarque, J. F., Lawrence, M. G., Montanaro, V., Muller, J. F., Pitari, G., Prather, M. J., Pyle, J. A., Rast, S., Rodriguez, J. M., Sanderson, M. G., Savage, N. H., Shindell, D. T., Strahan, S. E., Sudo, K., and Szopa, S.: Multimodel ensemble simulations of present-day and near-future tropospheric ozone, J. Geophys. Res.-Atmos., 111, D08301, doi:10.1029/2005jd006338, 2006.

van der Werf, G. R., Randerson, J. T., Giglio, L., Collatz, G. J., Kasibhatla, P. S., and Arellano, A. F.: Interannual variability in global biomass burning emissions from 1997 to 2004, Atmos. Chem. Phys., 6, 3423–3441, doi:10.5194/acp-6-3423-2006, 2006.

Vieno, M., Dore, A. J., Stevenson, D. S., Doherty, R., Heal, M. R., Reis, S., Hallsworth, S., Tarrason, L., Wind, P., Fowler, D., Simpson, D., and Sutton, M. A.: Modelling surface ozone during the 2003 heat-wave in the UK, Atmos. Chem. Phys., 10, 7963–7978, doi:10.5194/acp-10-7963-2010, 2010.

Vigouroux, C., De Maziere, M., Demoulin, P., Servais, C., Hase, F., Blumenstock, T., Kramer, I., Schneider, M., Mellqvist, J., Strandberg, A., Velazco, V., Notholt, J., Sussmann, R., Stremme, W., Rockmann, A., Gardiner, T., Coleman, M., and Woods, P.: Evaluation of tropospheric and stratospheric ozone trends over Western Europe from ground-based FTIR network observations, Atmos. Chem. Phys., 8, 6865–6886, doi:10.5194/acp-8-6365-2008, 2008.

Warneck, P.: Chemistry of the natural atmosphere, 2nd ed., This is volume 71 in the International geophysics series, Academic Press, San Diego, USA, 17, 927 pp., 2000.

Xiao, Y. P., Logan, J. A., Jacob, D. J., Hudman, R. C., Yantosca, R., and Blake, D. R.: Global budget of ethane and regional constraints on US sources, J. Geophys. Res.-Atmos., 113, D21306, doi:10.1029/2007jd009415, 2008.

Yurganov, L. N., Blumenstock, T., Grechko, E. I., Hase, F., Hyer, E. J., Kasischke, E. S., Koike, M., Kondo, Y., Kramer, I., Leung, F. Y., Mahieu, E., Mellqvist, J., Notholt, J., Novelli, P. C., Rinsland, C. P., Scheel, H. E., Schulz, A., Strandberg, A., Sussmann, R., Tanimoto, H., Velazco, V., Zander, R., and Zhao, Y.: A quantitative assessment of the 1998 carbon monoxide emission anomaly in the Northern Hemisphere based on total column and surface concentration measurements, J. Geophys. Res.-Atmos., 109, D15305, doi:10.1029/2004jd004559, 2004.

Yurganov, L. N., Duchatelet, P., Dzhola, A. V., Edwards, D. P., Hase, F., Kramer, I., Mahieu, E., Mellqvist, J., Notholt, J., Novelli, P. C., Rockmann, A., Scheel, H. E., Schneider, M.,

ACPD
11, 13723–13767, 2011

Schulz, A., Strandberg, A., Sussmann, R., Tanimoto, H., Velazco, V., Drummond, J. R., and Gille, J. C.: Increased Northern Hemispheric carbon monoxide burden in the troposphere in 2002 and 2003 detected from the ground and from space, Atmos. Chem. Phys., 5, 563–573, doi:10.5194/acp-5-563-2005, 2005.

Zhao, Y., Strong, K., Kondo, Y., Koike, M., Matsumi, Y., Irie, H., Rinsland, C. P., Jones, N. B., Suzuki, K., Nakajima, H., Nakane, H., and Murata, I.: Spectroscopic measurements of tropospheric CO, C_2H_6, C_2H_2,and HCN in northern Japan, J. Geophys. Res.-Atmos., 107, 4343, doi:10.1029/2001jd000748, 2002.

ACPD

11, 13723–13767, 2011

Table 1. Global sources of CO and C_2H_6 ($Tg\,yr^{-1}$). CO data are from Holloway et al. (2000) and C_2H_6 data are from Xiao et al. (2008).

	CO		C_2H_6	
Source	$Tg\,yr^{-1}$	%	$Tg\,yr^{-1}$	%
Anthropogenic*	408 (130–893)	15.1	8.5 (5–10.6)	64.9
Biomass burning	621 (310–920)	23.1	3.3 (1.3–6.4)	25.2
Biogenic hydrocarbon oxidation	530 (290–683)	19.7	Not a source	
Methane oxidation	910 (722–1459)	33.8	Not a source	
Biological processes	225 (0–756)	8.4	1.3	9.9
Total	2694 (1452–4711)	100	13.1 (6.3–17.0)	100

* Including: combustion, production and transportation of fossil fuels and combustion of bio-fuels

ACPD
11, 13723–13767, 2011

Table 2. Ground-based solar FTIR stations participating in the EMEP model comparison with available time period and number of measurements for each species.

Station	Latitude (° N)	Longitude (° E)	Altitude (m a.s.l.)	Retrieval code	Time period of data	Number CO	Number C_2H_6
Jungfraujoch	46.6	8.0	3580	SFIT2	1996–2006	1146	1175
Zugspitze	47.4	11.0	2960	SFIT2	1996–2006	736	671
Bremen	53.1	8.1	10	SFIT2	2002–2006	129	46
Harestua	60.2	10.8	600	SFIT2	1996–2006	458	507
Kiruna	67.8	20.4	420	PROFFIT	1996–2006	614	881
Ny-Ålesund	78.6	11.6	10	SFIT2	1996–2006	287	301

ACPD
11, 13723–13767, 2011

Table 3. EMEP model versions and sensitivity scenarios used in this paper.

EMEP model versions	Short name
European model	E
Global model	G
Global model with convection	Gc
As Gc but with forest fire module	Gcff
Sensitivity scenarios (based on the Gc model version)	**Short name**
20 % reduction of European anthropogenic CO	GcEUR20
20 % reduction of North American anthropogenic CO	GcNA20
20 % increase of East Asian anthropogenic CO	GcEA20
20 % reduction of all European emissions	GcEURAll20
20 % reduction of all North American emissions	GcNAAll20
20 % reduction of all East Asian emissions	GcEAAll20
0.2 °C increase of the global temperature	GcT0.2
1.2 % increase of global CH_4	Gc$CH_4$1.2
100 % reduction of North American BVOC	Gcnobvoc

ACPD
11, 13723–13767, 2011

Table 4. Average values (μ), standard deviations (σ) and seasonal amplitudes (A) from the FTIR measurements and European-scale model (E). A is the difference between the average values of March and April and July to September.

	CO (molecules $cm^{-2} \times 10^{17}$)						C_2H_6 (molecules $cm^{-2} \times 10^{15}$)					
	FTIR			E			FTIR			E		
	μ	σ	A	μ	σ	A	μ	σ	A	μ	σ	A
Jungfraujoch	11.1	1.6	1.4	10.0	1.9	1.9	10.7	2.7	2.5	12.5	4.7	5.6
Zugspitze	12.6	1.8	1.6	11.0	2.1	2.0	12.5	3.0	2.9	14.2	5.2	6.3
Bremen	21.5	3.5	2.9	18.1	3.6	3.5	17.6	5.1	5.1	22.6	10.0	10.4
Harestua	21.0	3.0	3.1	17.8	3.1	3.3	23.4	6.4	7.1	25.8	7.8	9.5
Kiruna	21.2	3.5	3.2	17.0	3.5	3.4	30.6	11.4	11.0	24.2	9.3	10.0
Ny-Ålesund	20.6	4.0	3.8	16.3	2.9	3.3	18.4	5.5	6.0	24.1	8.2	9.7

ACPD
11, 13723–13767, 2011

Table 5. Average (μ) and standard deviation (σ) contribution from the boundary conditions (BIC) for the European-scale EMEP model, expressed in percent (%).

	CO		C_2H_6	
	μ	σ	μ	σ
Jungfraujoch	65.8	18.4	76.2	14.8
Zugspitze	61.4	15.6	74.4	12.6
Bremen	60.8	15.5	71.2	14.3
Harstua	72.5	14.8	78.5	14.1
Kiruna	87.6	12.5	91.8	9.7
Ny-Ålesund	96.6	5.1	98.2	3.6

ACPD
11, 13723–13767, 2011

Table 6. Linear trends estimated from the partial columns (below 100 hPa) of CO and C_2H_6 from FTIR measurements. The trends are presented with their 2-σ confidence intervals and used the average value of 2001 as reference.

Station	Time period	FTIR trends (% yr^{-1})	
		CO	C_2H_6
Jungfraujoch	(1996–2006)	−0.45±0.16	−1.51±0.23
Jungfraujoch	(1998–2006)	−1.32±0.20	−2.14±0.29
Zugspitze*	(1996–2006)	−1.00±0.24	−2.11±0.30
Zugspitze	(1998–2006)	−1.16±0.26	−2.25±0.35
Harestua	(1996–2006)	−0.62±0.19	−1.09±0.25
Kiruna	(1996–2006)	−0.61±0.16	−1.15±0.18

* No CO data is available for Zugspitze from September 1996 to June 1997.

ACPD
11, 13723–13767, 2011

Table 7. Average values (μ) from March to December for the global (Gc) and European-scale (E) model and FTIR measurements. January and February data are excluded from the μ values because of the high influence from the start conditions in the global model.

	CO μ (molecules cm^{-2} × 10^{18})			C_2H_6 μ (molecules cm^{-2} × 10^{15})		
	FTIR	Gc	E	FTIR	Gc	E
Jungfraujoch	1.0	1.0	1.1	12.4	7.5	9.8
Zugspitze	1.1	1.2	1.2	14.2	9.0	11.6
Bremen	1.8	1.7	2.0	21.9	11.0	16.9
Harestua	1.6	1.6	1.9	21.9	12.9	18.9
Kiruna	1.6	1.6	2.0	23.3	13.6	27.9
Ny-Ålesund	1.8	1.7	2.1	29.9	17.7	21.9

ACPD
11, 13723–13767, 2011

Table 8. Change in the CO partial column per year through the 1996-2006 time period. All the simulations are done on year 2006 and are scaled to represent the yearly change.

	Sensitivity cases ($\%\,yr^{-1}$)						
	GcEUR20	GcEA20	GcNA20	$GcCH_4$1.2	GcT0.2	ΣGc	FTIR
Jungfraujoch	−0.47	0.15	−0.22	0.13	0.04	−0.37	−0.45±0.16
Zugspitze	−0.58	0.15	−0.21	0.13	0.04	−0.47	−1.00±0.24
Bremen	−0.83	0.15	−0.21	0.13	0.04	−0.72	N/A
Harestua	−0.67	0.16	−0.21	0.13	0.04	−0.55	−0.62±0.19
Kiruna	−0.60	0.16	−0.21	0.12	0.04	−0.49	−0.61±0.16
Ny-Ålesund	−0.53	0.18	−0.20	0.12	0.04	−0.39	N/A

ACPD
11, 13723–13767, 2011

Table 9. Modeled trends at ground level and adjusted altitude.

	Sensitivity cases (% yr^{-1})	
	ΣGc altitude adjusted	ΣGc ground level
Jungfraujoch	−0.37	−0.60
Zugspitze	−0.47	−0.67

ACPD
11, 13723–13767, 2011

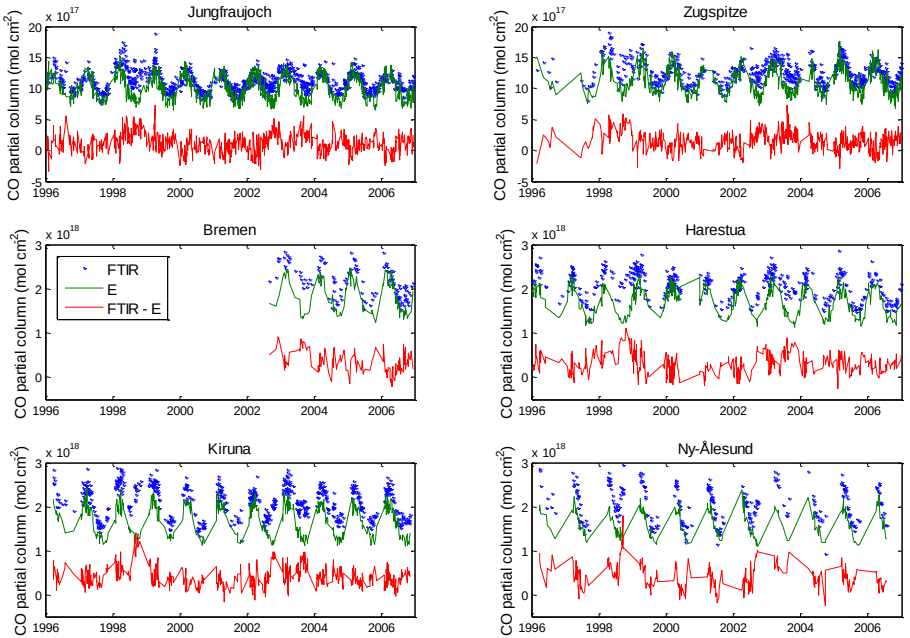

Fig. 1. CO comparison between European EMEP model (E) and FTIR measurements. The measurements are marked as dots and the model is marked as a solid green line. The difference between measurements and model are marked as a red solid line.

ACPD
11, 13723–13767, 2011

CO and C_2H_6 trends from ground-based solar FTIR measurements

J. Angelbratt et al.

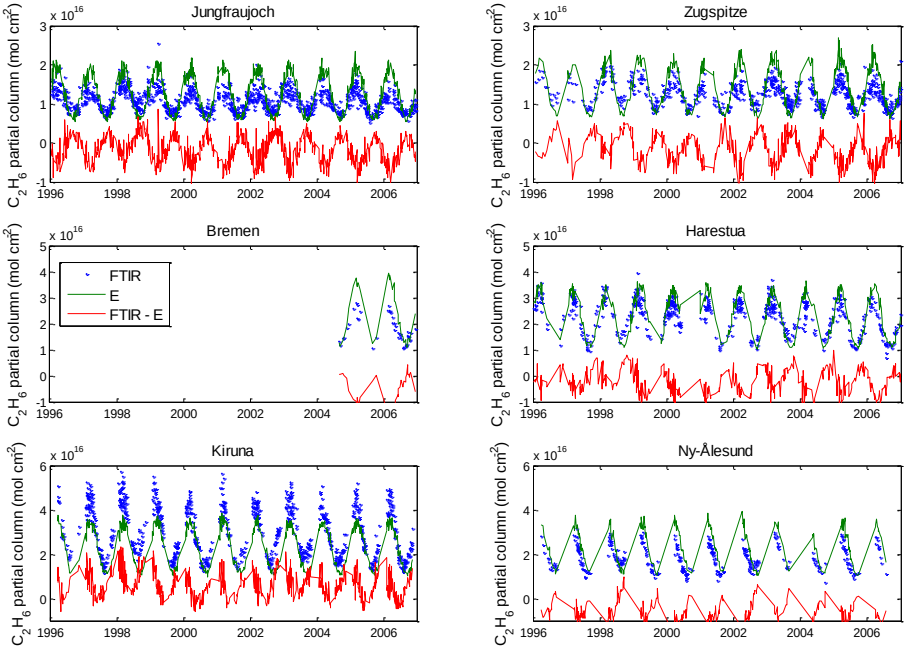

Fig. 2. As in Fig. 1 but for C_2H_6.

ACPD
11, 13723–13767, 2011

CO and C_2H_6 trends from ground-based solar FTIR measurements

J. Angelbratt et al.

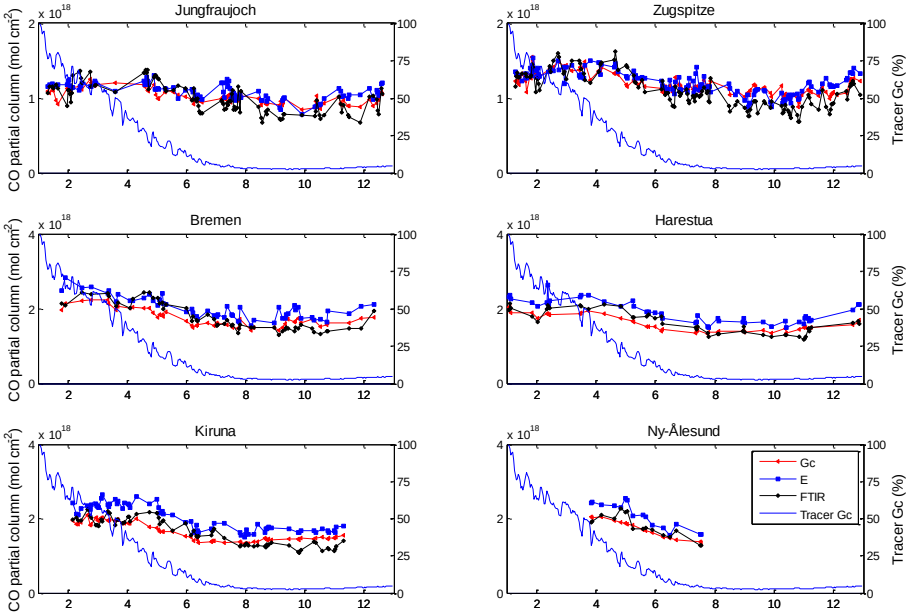

Fig. 3. CO partial columns derived from the global (triangles) and European-scale (squares) EMEP model. The tracers (solid line) and FTIR (diamonds) data is also shown in the figures. The first months are highly influenced by the model start conditions but decreases rapidly with time. This corresponds well to the CO and C_2H_6 lifetimes of 2-3 months given in the literature by (Finlayson-Pitts and Pitts, 2000).

ACPD
11, 13723–13767, 2011

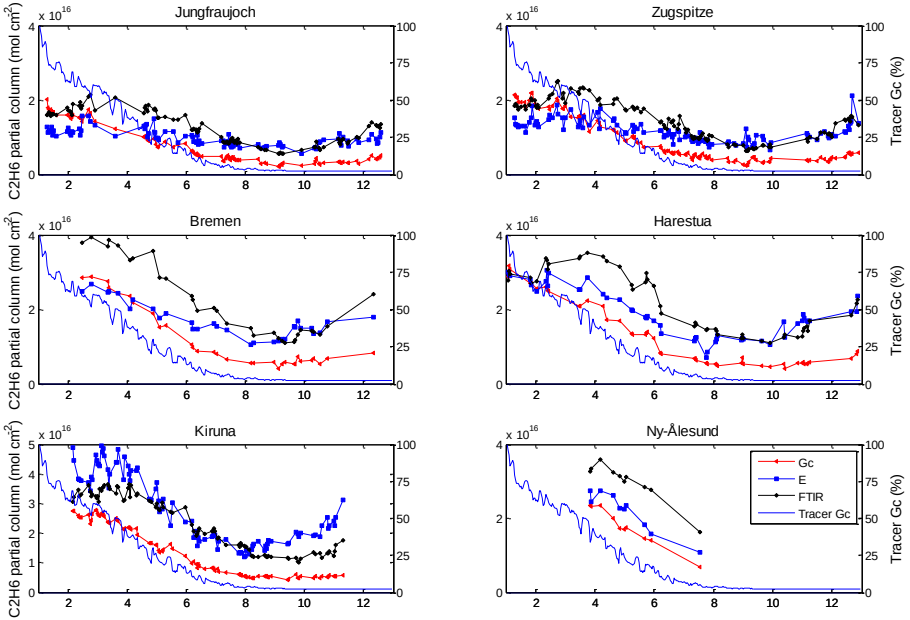

Fig. 4. As figure 3 but for C_2H_6.

ACPD
11, 13723–13767, 2011

CO and C_2H_6 trends from ground-based solar FTIR measurements

J. Angelbratt et al.

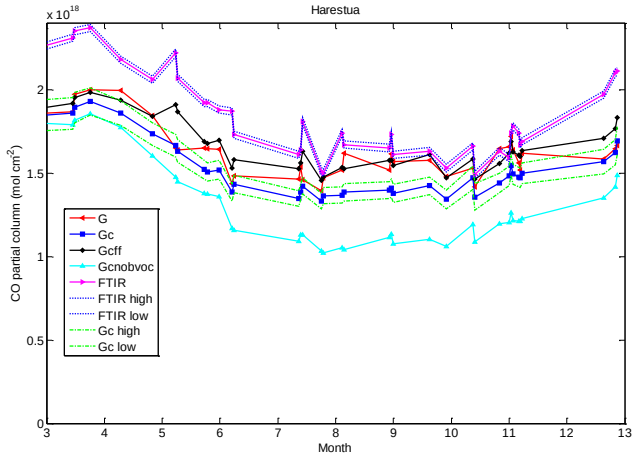

Fig. 5. Global EMEP model versions and FTIR measurements for Harestua.

ACPD
11, 13723–13767, 2011

CO and C_2H_6 trends from ground-based solar FTIR measurements

J. Angelbratt et al.